PROCEEDINGS of the
23rd International Congress on Acoustics

9 to 13 September 2019 in Aachen, Germany

Thermoacoustic instabilities: physical mechanisms and mathematical modelling

Maria HECKL

School of Chemical and Physical Sciences, Keele University, U.K.

m.a.heckl@keele.ac.uk

ABSTRACT

If a flame is put into an acoustic resonator, an escalating interaction between the flame's heat release and the acoustic field can occur, giving rise to intense pressure oscillations. This phenomenon is termed "thermoacoustic instability". It occurs in combustion systems that have a continuously burning flame, such as gas turbines, jet aeroengines, boiler and heating systems, furnaces and rockets. Thermoacoustic instabilities are a serious problem because they can lead to excessive structural vibrations, fatigue, and even catastrophic hardware damage. The escalating flame-sound interaction occurs in tandem with other physical mechanisms, leading to a complex web of interactions, most of which are nonlinear. They include flame-vortex interactions, flame response to fluctuations in fuel concentration, entropy waves, flame-structure interactions, and others.

The development of low-pollution combustion systems is very important for our environment. However, such combustion systems are particularly prone to thermoacoustic instabilities. Progress with developing combustion systems that are immune to these is hampered by insufficient physical insight. Efforts to gain further insight are going on by researchers worldwide using experimental, analytical and numerical tools. This talk aims to give an overview of the key physical mechanisms involved in thermoacoustic instabilities and will present mathematical modelling approaches inspired by physical insight.

Keywords: flame models, tailored Green's function, low-pollution combustion systems

1. INTRODUCTION

The most basic thermoacoustic system is a Rijke tube [1,2]. It is an open-ended tube, held vertically, with a horizontal wire gauze in the lower half of the tube. If the gauze is sufficiently hot, the tube emits a loud sound, typically at a frequency that corresponds to the fundamental mode of the tube. This sound is generated by thermoacoustic feedback, which is the interaction between the following two processes:
(1) The heat release rate of the hot gauze fluctuates, leading to fluctuations in density and temperature of the air surrounding it; as a consequence, a sound wave is generated.
(2) The sound wave impinges on the hot gauze, leading to oscillations in the air flow and hence in the heat transfer rate; as a consequence, the heat release rate from the hot gauze fluctuates.

A feedback loop between these two processes is established because any sound waves generated by the hot gauze are reflected at the tube ends back into the tube and towards the flame. This is shown schematically in Figure 1.

Figure 1 – Feedback between hot gauze and sound field

An example of an escalating thermoacoustic feedback, i.e. a thermoacoustic instability, can be seen in Figure 2, which shows the time history of the pressure in a Rijke tube [3, p. 49]. At first, the pressure amplitude increases exponentially (as indicated by the dashed line), then it grows less rapidly, and eventually the amplitude reaches a constant value.

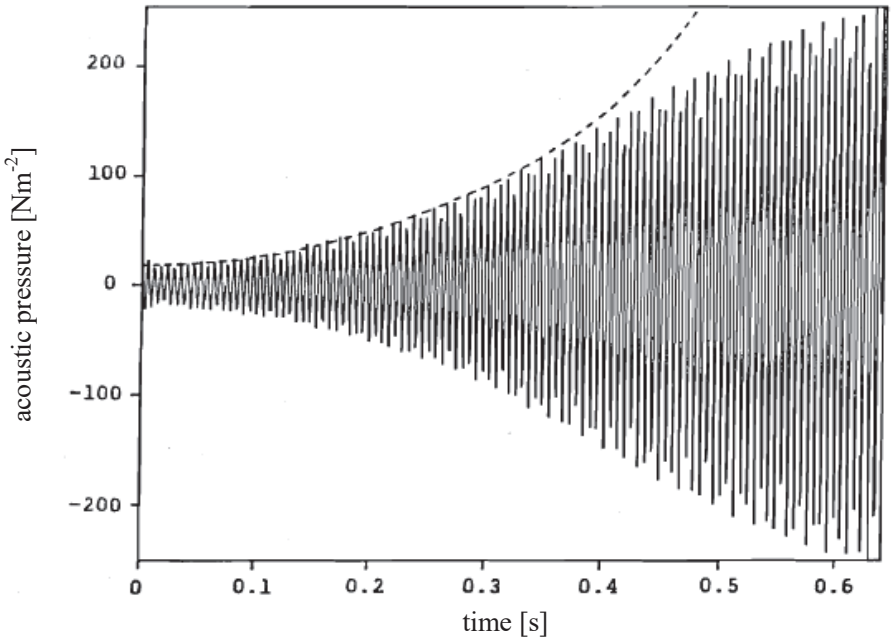

Figure 2 – Time history of the acoustic pressure during a thermoacoustic instability in a Rijke tube

This thermoacoustic feedback occurs not only in the Rijke tube, but more importantly in any acoustic resonator, which houses a flame that responds to fluctuations in the surrounding flow field. This includes all combustion systems that have a continuously burning flame, such as gas turbine engines, jet aeroengines, boiler and heating systems, furnaces and rockets. Here, the basic instability mechanism is also a thermoacoustic feedback loop. This, however, does not occur in isolation, but is coupled with other physical mechanisms, leading to a complex web of interaction, which tend to be nonlinear.

Combustion is responsible for a number of pollutants of the environment, in particular NO_x and CO_2. In order to minimise NO_x production, green combustion technologies use lean premixed flames and burn at low temperatures. CO_2 production can be minimised by adding hydrogen to the fuel and/or using biofuels. Unfortunately, combustion systems based on these approaches are particularly prone to thermoacoustic instabilities. These can occur suddenly and spontaneously, and when they occur, the resulting oscillations may be so violent that they cause structural damage; for example, Goy et al [4, chapter 4] report the destruction of a combustion liner and a burner assembly.

Progress with developing combustion systems that are immune to thermoacoustic instabilities is hampered by insufficient physical insight. Efforts to gain new insight are made by researchers worldwide, using experimental, analytical and numerical approaches. One can get an overview in the review articles of Candel [5], Lieuwen [6] and Huang & Yang [7], in the books by Lieuwen & Yang [4] and Poinsot & Veynante [8], in the text by Culick [9], and in the recent review paper by Heckl [10].

The aim of this paper is to consider a generic combustion system, to describe the most important physical processes that occur in it, and to explain how these can be modelled mathematically. The paper is structured as follows. Section 2 will give an overview of the key physical mechanisms involved in thermoacoustic instabilities. Section 3 will introduce a new method to model linear and nonlinear flames mathematically. The advantages of using the tailored Green's function for thermoacoustic modelling purposes will be demonstrated in Section 4. Section 5 will present a case study, where the concepts from Sections 3 and 4 are applied. Conclusions will be given in Section 6.

2. PHYSICAL MECHANISMS

We consider a generic combustion system, as shown in Figure 3(a). It comprises a mixing tube, a combustion chamber and an exhaust nozzle. Air and fuel enter the upstream end of the mixing tube through separate inlets. They mix as they move downstream, and form a more or less homogeneous mixture that enters the combustion chamber as a jet. The shear layer surrounding the jet is unstable; this leads to the formation of vortices, which are shed periodically, as illustrated in Figure 3(b). The flame, which is anchored near the upstream end of the combustion chamber, is perturbed by the vortices; its surface area fluctuates, and as a consequence, the rate of heat release fluctuates; this is shown in Figure 3(c). As explained in Section 1, a heat source with a fluctuating rate of heat release acts as a sound source. Hence the flame emits acoustic waves, which travel away from either side of the flame, see Figure 3(d). The acoustic waves are reflected at the resonator boundaries and form a standing wave with a frequency that is close to one of the resonance frequencies of the combustion system.

The acoustic wave induces several secondary feedback loops:

(1) One of these involves mixture inhomogeneities, which are generated because the oscillating pressure in the mixing tube modulates the air flow and/or fuel flow. This leads to perturbations in the equivalence ratio ϕ. These are swept by the mean flow towards the flame, where they induce further fluctuations in the heat release rate. This establishes a feedback loop, where the ϕ fluctuations travel with the bulk flow – at low Mach number – from the air/fuel inlet to the flame, and the sound waves travel in the opposite direction with the speed of sound, from the flame to the air/fuel inlet; Figure 4(a) illustrates this.

(2) Another secondary feedback loop involves modulations of the flow of the premix, which are generated by the oscillating pressure at the combustion chamber inlet. The modulated flow perturbs the heat release rate of the flame, which in turn creates a new sound wave. In this feedback loop, the flow modulations travel with a speed similar to that of the mean flow from the combustion chamber inlet to the flame, and the sound waves travel with the speed of sound in the opposite direction from the flame to the combustion chamber inlet, see Figure 4(b).

(3) A further secondary feedback loop involves vortices, which are generated upstream of the flame, typically at a sharp edge that forms part of the flame holder. The velocity fluctuations imposed by the sound wave at the sharp edge synchronises the vortex shedding. This establishes a feedback loop, where vortices travel the length of the flame and on their way disturb the surface area and heat release rate of the flame. The flame responds by generating a sound wave, which reinforces the synchronised vortex shedding. The vortices travel with a speed similar to the mean flow in the combustion chamber from the base to the tip of the flame, and the sound waves travel with the speed of sound in the opposite direction. This is shown schematically in Figure 4(c).

Each of these three feedback loops are characterised by a frequency that is determined by the time it takes to complete one cycle of the loop. Given that the mean flow travels much more slowly than the sound wave, the time to complete one cycle is dominated by the speed of the mean flow. The periodic oscillations driven by these secondary feedback loops are termed "intrinsic modes"; they have received much attention recently [11, 12, 13]. Their frequencies are independent of the resonator frequencies. However, if the frequency of an intrinsic mode happens to be close to one of the resonator frequencies, coupling between an acoustic and intrinsic mode ensues, and they may adopt a common frequency. This phenomenon is called "lock-on" [14, 15].

Although the flame is the primary sound source in the combustion chamber, it may not be the *only* sound source. The following process can activate a secondary sound source: Apart from generating sound waves, an unsteady flame also generates hot-spots that are swept downstream towards the exhaust. These travelling hot-spots are called "entropy waves" [16, 17]; their propagation speed is similar to that of the mean flow. As long as the hot-spots travel with a constant speed, they produce no sound. However, if they are accelerated, which happens when they pass through a constriction (e.g. the exhaust nozzle or through the gap between turbine blades) they turn into a sound source. A new feedback loop ensues: a hot-spot travels from the flame to the exhaust where it gets accelerated; the sound waves generated by this process travel from the nozzle back to the flame, where they disturb the heat release rate and induce yet more hot-spots. Figure 4(d) visualises this feedback loop.

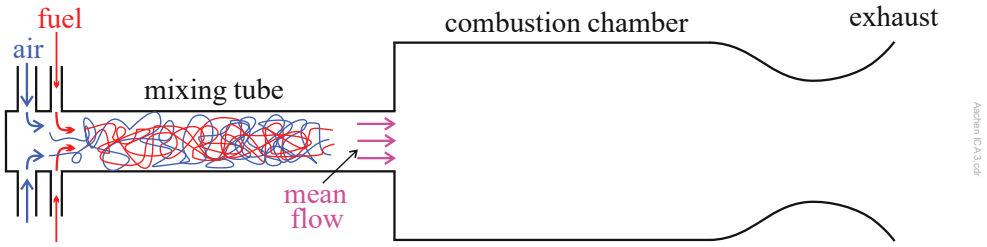

Figure 3(a) – Mixing of fuel and air to form a premix travelling with constant speed (the mean flow speed).

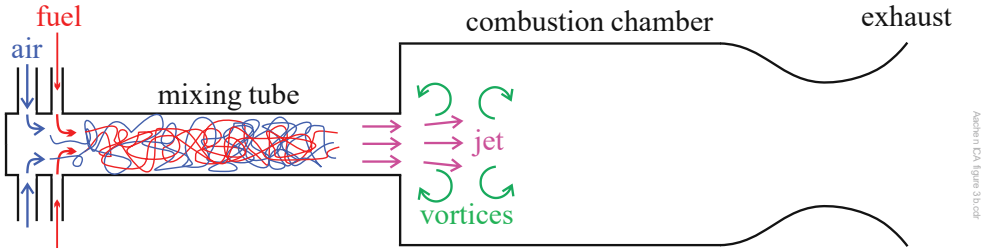

Figure 3(b) – Vortex shedding near the upstream end of the combustion chamber

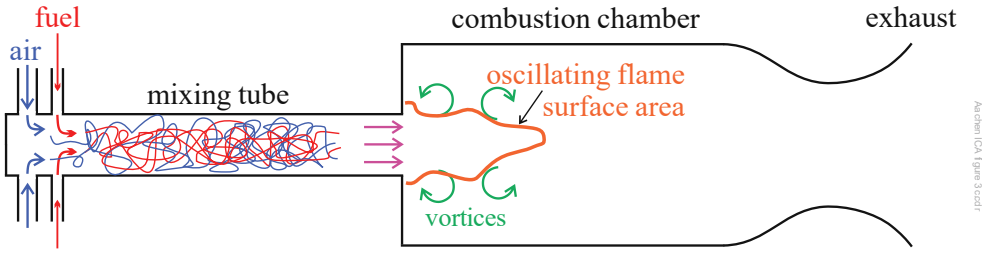

Figure 3(c) – Fluctuations of the flame surface area induced by vortices

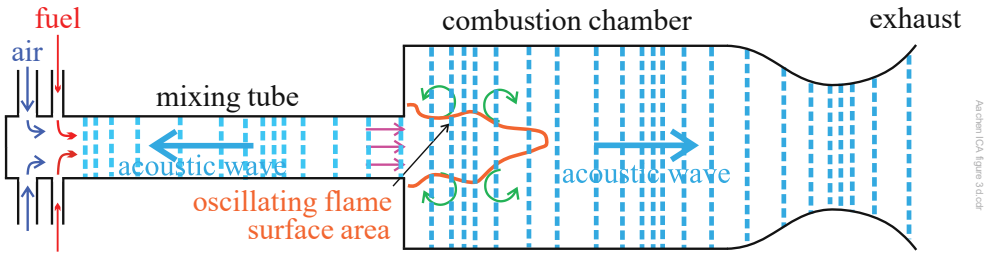

Figure 3(d) – Generation of acoustic waves travelling towards the boundaries of the combustion system

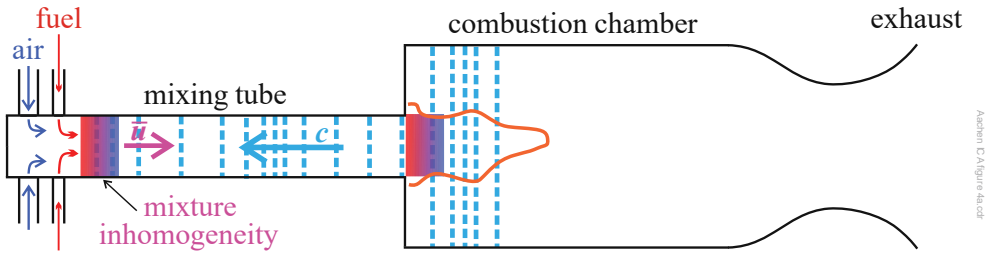

Figure 4(a) – Feedback loop formed by right-travelling mixture inhomogeneities (speed similar to $\bar{u}$) and left-travelling sound waves (speed c)

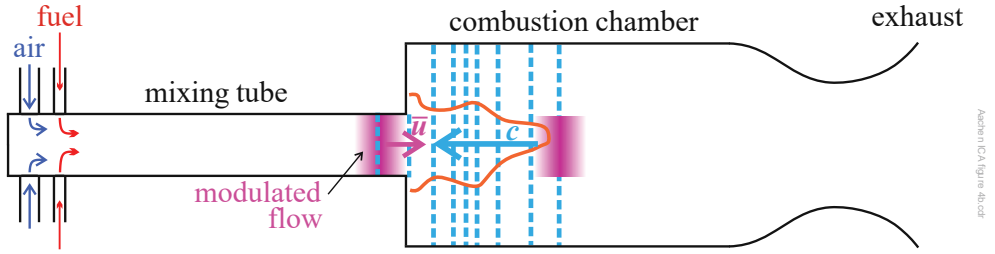

Figure 4(b) – Feedback loop formed by right-travelling flow modulations (speed similar to $\bar{u}$) and left-travelling sound waves (speed c)

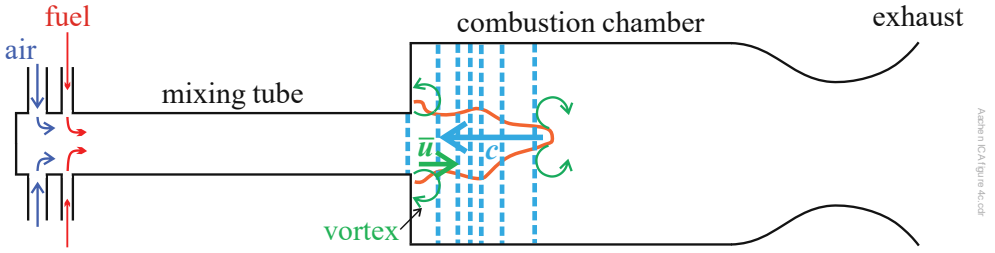

Figure 4(c) – Feedback loop formed by right-travelling vortices (speed similar to $\bar{u}$) and left-travelling sound waves (speed c)

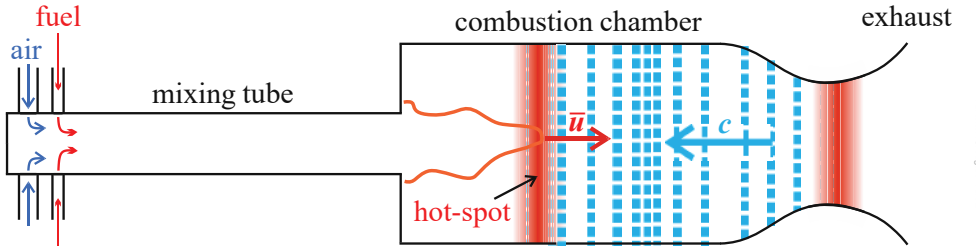

Figure 4(d) – Feedback loop formed by right-travelling hot-spots (speed similar to $\bar{u}$) and left-travelling sound waves (speed c)

All the feedback mechanisms illustrated in Figure 4 combine to form a web of multiple interactions. They may be supplemented by further interactions: a swirler (typically near the downstream end of the mixing tube) would generate a flow field with different velocity components; a row of heat exchanger tubes would act as a heat sink and also redistribute the acoustic field; flexible combustion chamber walls would be able to vibrate and so absorb acoustic energy from the sound field.

3. MATHEMATICAL MODELLING OF FLAMES

For low-order modelling of a combustion system, the flame is considered as an input-output system and described in the frequency (ω) domain. The input is a velocity fluctuation, $\hat{u}(\omega)$, and the output is a fluctuation in the heat release rate, $\hat{Q}(\omega)$ (the hat $\hat{}$ denotes complex amplitudes). The flame is described by the flame transfer function (FTF), denoted here by $\mathcal{T}(\omega)$ and defined by

$$\mathcal{T}(\omega) = \frac{\hat{Q}(\omega)/\bar{Q}}{\hat{u}(\omega)/\bar{u}}, \tag{1}$$

where $\bar{Q}$ is the mean heat release rate and $\bar{u}$ is the speed of the mean flow. The FTF can be measured by the setup shown in Figure 5.

Figure 5 – Setup to measure the FTF

The mean flow $\bar{u}$ gives rise to the mean heat release rate $\bar{Q}$. The oscillating velocity comes from an external source (e.g. a loudspeaker); it excites the flame with velocity $\hat{u}(\omega)$ and induces fluctuations $\hat{Q}(\omega)$ in the heat release rate. $\hat{Q}(\omega)$ is measured indirectly from the light emitted by a particular radical produced during the chemical reaction. The frequency ω is varied during the measurement in the required range. Figure 6 shows a typical result for the gain, $|\mathcal{T}(\omega)|$, and phase, $\angle\mathcal{T}(\omega)$, of a premixed flame.

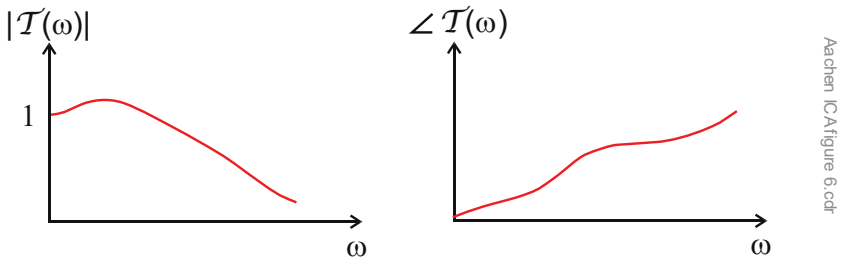

Figure 6 – Typical spectrum for the gain and phase of a FTF.

If the inverse Fourier transform is applied to Eq. (1), the following result is obtained,

$$\frac{Q'(t)}{\bar{Q}} = \int_{-\infty}^{\infty} h(\tau)\frac{u'(t-\tau)}{\bar{u}}\,\mathrm{d}\tau, \tag{2}$$

where $h(\tau)$ is the inverse Fourier transform of $\mathcal{T}(\omega)$. The dashes indicate time-domain quantities: Q' is the fluctuating part of the heat release rate in the time domain, and u' is the fluctuating part of the velocity.

The function $h(\tau)$ has a straightforward physical meaning: it is the impulse response of the flame, as can be seen easily by putting

$$u'(t) = \bar{u}\,\delta(t) \tag{3}$$

into Eq. (2). The FTF and the impulse response are mathematically equivalent, and therefore they contain exactly the same physical information: the FTF is the representation in the frequency domain, and the impulse response is the representation in the time domain. A typical result for $h(\tau)$ is shown in Figure 7.

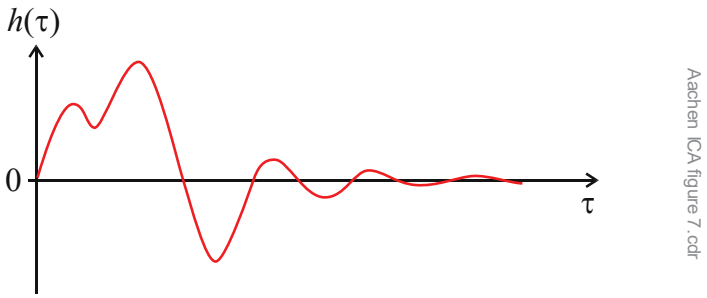

Figure 7 – Typical time history of a flame's impulse response

This time history has a succession of maxima and minima, which fade for large times. This is in line with the physical observations described in section 2: there are several feedback loops involving transport processes, and each of these transport processes introduces its own time delay. The maxima and minima in Figure 7 are not infinitesimally narrow, like the delta function in Eq. (3), but are surrounded by a distribution. The finite width of these distributions is due to various factors, such as dispersion during the transport processes (section 7 in [10]). A detailed analysis of the dispersion in one such transport process (swirl waves) has been made by Albayrak et al [18].

For mathematical modelling purposes, is useful to have an analytical representation of the FTF and impulse response of a given flame. A method has been developed by Gopinathan and Heckl [19], which exploits the fact that the individual maxima and minima in a flame's impulse response have the shape of a bell and so can be fitted with Gauss curves. Gopinathan and Heckl use a *superposition* of Gauss curves,

$$\tilde{h}(\tau) = \frac{n_1}{2\pi\sigma_1}\,\mathrm{e}^{-\frac{(\tau-\tau_1)^2}{2\sigma_1^2}} + \frac{n_2}{2\pi\sigma_2}\,\mathrm{e}^{-\frac{(\tau-\tau_2)^2}{2\sigma_2^2}} + \frac{n_3}{2\pi\sigma_3}\,\mathrm{e}^{-\frac{(\tau-\tau_3)^2}{2\sigma_3^2}} + \ldots \tag{4}$$

to approximate a given impulse response obtained from FTF data, which may come from numerical simulations or experimental measurement. The following quantities are treated as fitting parameters and determined numerically from a nonlinear least-square fitting routine:

n_j - measure for the height of the Gauss curve; this can be positive (maximum) or negative (minimum)

τ_j - position of the centre of the Gauss curve along the time axis, i.e. prominent time-lag

σ_j - width of the Gauss curve

The integer $j = 1, 2, 3, \ldots$ denotes the *j*th Gauss curve in the sum in Eq. (4).

The frequency-domain equivalent of Eq. (4) is the Fourier transform, which can be evaluated analytically. The result is

$$\tilde{\mathcal{T}}(\omega) = n_1 \mathrm{e}^{-\frac{\omega^2\sigma_1^2}{2}}\mathrm{e}^{\mathrm{i}\omega\tau_1} + n_2 \mathrm{e}^{-\frac{\omega^2\sigma_2^2}{2}}\mathrm{e}^{\mathrm{i}\omega\tau_2} + n_3 \mathrm{e}^{-\frac{\omega^2\sigma_3^2}{2}}\mathrm{e}^{\mathrm{i}\omega\tau_3} + \ldots\,. \tag{5}$$

The approach described here is a physically motivated mathematical tool to represent a set of FTF data points by analytical expressions for the FTF and its corresponding impulse response. These expressions involve a small number of fitting parameters (typically 6 or 9), which are the same in the frequency domain and in the time domain.

The concept of the FTF has been extended into the nonlinear regime by Noiray et al [20]. They measured the FTF with input signals $\hat{u}(\omega)$ of several velocity amplitudes, denoted here by a, and so obtained an amplitude-dependent FTF, called "flame describing function" (FDF),

$$\mathcal{T}(\omega, a) = \frac{\hat{Q}(\omega, a) / \bar{Q}}{\hat{u}(\omega, a) / \bar{u}} . \tag{6}$$

Just like its linear equivalent, the FDF can be represented analytically by a superposition of Gauss curves as described above. The fitting parameters n_j, τ_j, σ_j ($j = 1, 2, 3, \ldots$) then become amplitude-dependent. An example is shown in Figures 8, 9 and 10 below. These figures are for a methane-hydrogen flame (80% CH_4, 20% H_2) with an equivalence ratio of 0.95. Figure 8 shows the gain and phase of the FDF; the markers indicate the original data, and the solid curves give the corresponding analytical representations, using three Gauss curves. The following five amplitudes are shown: $\varepsilon = a / \bar{u} = 0.02, 0.04, 0.06, 0.08, 0.1$. Figure 9 shows the corresponding inverse Fourier transforms; the dashed curves are for the inverse Fourier transforms of the original data, and the solid curves denote the corresponding analytical representations. The curves are extremely similar and hard to distinguish from one another. Figure 10 illustrates the amplitude-dependence of the fitting parameters (the amplitude range depicted here includes higher values that are not shown in Figures 8 and 9).

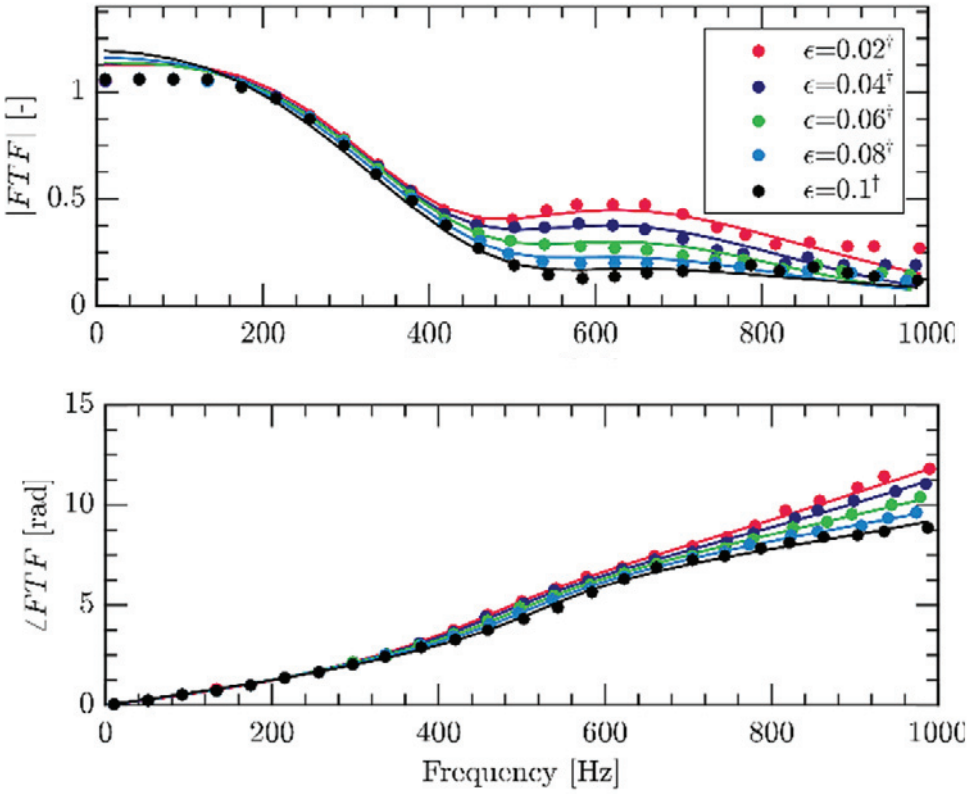

Figure 8 – Gain and phase of the FDF of a CH_4 - H_2 flame. Markers: original data from numerical simulation. Solid curves: analytical representations (from [19]).

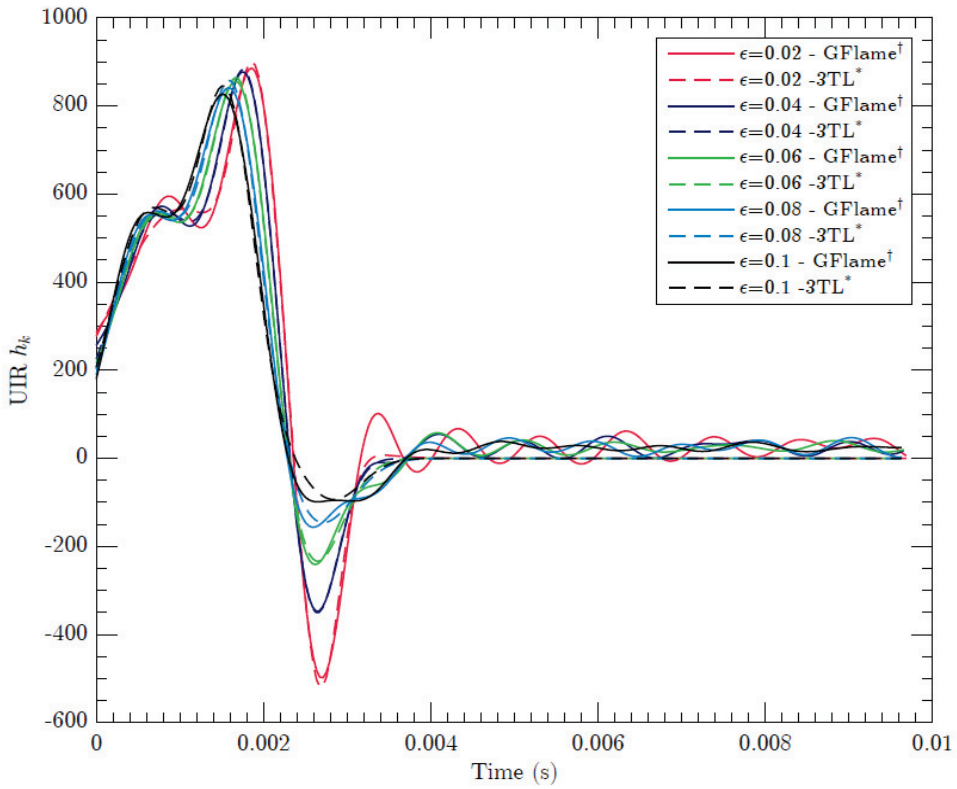

Figure 9 – Inverse Fourier transform of the FDF in Figure 8. Dashed curves: inverse Fourier transform of the original FDF data. Solid curves: analytical representations (from [19]).

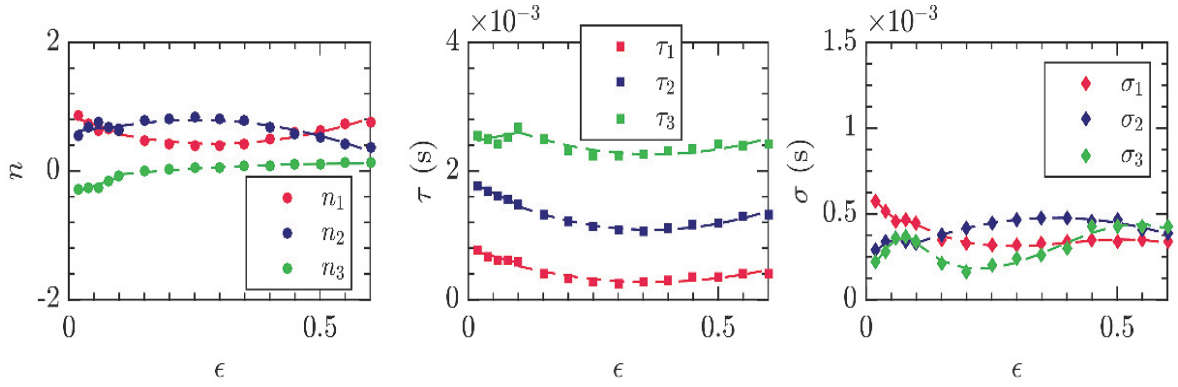

Figure 10 – Amplitude-dependence of the fitting parameters for the CH_4 - H_2 flame in Figures 8 and 9 (from [19]).

4. THERMOACOUSTIC MODELLING WITH THE TAILORED GREEN'S FUNCTION

The Green's function is an impulse response. In an acoustic context, it is the response to a point source at position $\vec{x}*$, emitting an impulsive sound signal at time $t*$, measured by an observer at position $\vec{x}$ at time t. The *tailored* Green's function is the response in a configuration, where the source and observer are both inside an acoustic resonator. We denote the Green's function by $G(\vec{x},\vec{x}*,t-t*)$. Its governing equation is the nonhomogeneous wave equation,

$$\frac{1}{c^2}\frac{\partial^2 G}{\partial t^2}-\nabla^2 G=\delta(\vec{x}-\vec{x}*)\delta(t-t*)\,, \tag{7}$$

where c is the speed of sound. It also has to satisfy the boundary conditions of the acoustic resonator, as well as the causality condition

$$G(\vec{x},\vec{x}*,t-t*)=0 \quad \text{for} \quad t<t*\,. \tag{8}$$

The general form of the tailored Green's function is a superposition of resonator modes; for a 1-D geometry, this can be written as

$$G(x,x*,t-t*)=\mathrm{H}(t-t*)\sum_{n=1}^{\infty} G_n(x,x*)\,\mathrm{e}^{-\mathrm{i}\omega_n(t-t*)}\,, \tag{9}$$

where n is the mode number, H is the Heaviside function (this guarantees that the causality condition (8) is satisfied), ω_n is the frequency (which may be complex with a negative imaginary part if the mode is damped) of mode n, and $G_n(x,x*)$ is its amplitude. ω_n and $G_n(x,x*)$ can be calculated analytically for configurations, that can be divided into uniform 1-D sections; in principle, they can also be measured.

The tailored Green's function is a useful mathematical tool for the solution of partial differential equations (PDE) that have a forcing term. One such PDE is the acoustic analogy equation [21],

$$\frac{1}{c^2}\frac{\partial^2 \varphi}{\partial t^2}-\nabla^2\varphi=-\frac{\overline{\rho}(\gamma-1)}{c^2}\frac{\partial q'}{\partial t}\,, \tag{10}$$

written here for the velocity potential φ. The left hand side is the well-known part of the standard wave equation, while the right hand side represents the forcing term. This contains the quantity q', which is the fluctuating part of the local heat release rate (heat release rate per unit mass); the quantities $\overline{\rho}$ (mean density) and γ (specific heat ratio) are constants.

Equation (10) expresses the fact (mentioned in the second paragraph of the introduction) that a heat source with a fluctuating rate of heat release is a source of sound. By combining the two PDEs (7) and (10), and assuming that the flame is compact, i.e. its heat release rate can be described by

$$q'(\vec{x},t)=q(t)\delta(\vec{x}-\vec{x}_q)\,, \tag{11}$$

an integral equation can be derived for the acoustic field. This derivation involves several mathematical steps, which can be found in [22]. The resulting equation for the 1-D case is

$$u'_q(t)=-\frac{\gamma-1}{c^2}\int_{t*=0}^{t}\left.\frac{\partial G}{\partial x}\right|_{\substack{x=x_q\\ x'=x_q}} q(t*)\,\mathrm{d}t*\,, \tag{12}$$

where $u'_q(t)$ denotes the acoustic velocity at the flame position x_q. This equation can be interpreted in a straightforward manner. To this end, we write it in terms of the acoustic pressure p'_q at the flame position (omitting the constant term with $\overline{\rho}$ and γ),

$$p'_q(t)=\int_{t*=0}^{t} q(t*)\,G(t-t*)\,\mathrm{d}t*\,. \tag{13}$$

$G(t-t^*)$ is the Green's function, i.e. the response at time t to a unit impulse emitted at time t^*. Hence the response to an impulse emitted at t_1 with peak value q_1 is $q_1\,G(t-t_1)$. This is illustrated in the top two sub-figures of Figure 11. The response to an impulse emitted at t_2 with peak value q_2 is $q_2\,G(t-t_2)$, and so on. The time history of the source term $q(t^*)$ can be approximated by a series of impulses in quick succession, with varying peak values $q_1, q_2, \ldots$, as shown in the bottom left sub-figure of Figure 11. The responses to these individual impulses superimpose to form the combined response $q_1\,G(t-t_1)+q_2\,G(t-t_2)+\ldots$, as shown in the bottom right sub-figure. This sum is simply the discretized version of the integral in Eq. (13).

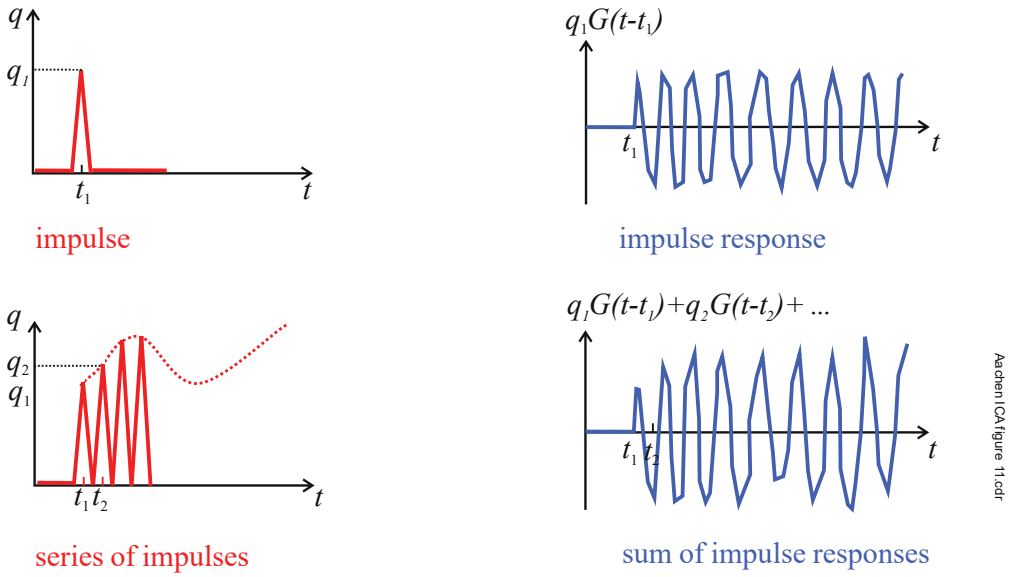

Figure 11 – Interpretation of the integral equation (13)

In order to be able to solve Eq. (12), it is necessary to know how the heat release rate depends on the acoustic field. A suitable flame model provides this information. We assume that it is given by a functional in the generic form

$$q(t) = \mathcal{F}(u_q(t))\,. \tag{14}$$

In the simplest case, (14) would be a time-lag law with coupling coefficient n and time-lag τ,

$$q(t) = n\,u_q(t-\tau)\,. \tag{15}$$

In the general case, the functional $\mathcal{F}$ can be determined from the FTF or FDF of a specific flame.

A governing integral equation for the velocity $u_q(t)$ is obtained by inserting (14) into the integrand of Eq. (12),

$$u'_q(t) = -\frac{\gamma-1}{c^2}\int_{t^*=0}^{t} \left.\frac{\partial G}{\partial x}\right|_{\substack{x=x_q \\ x'=x_q}} \mathcal{F}(u_q(t^*))\,\mathrm{d}t^*\,. \tag{16}$$

This equation can be solved numerically with a straightforward iteration, stepping forward in time; details can be found in Bigongiari and Heckl [23].

5. CASE STUDY: MODE COUPLING IN A HALF-WAVE RESONATOR WITH A NONLINEAR FLAME

The configuration in this case study is an open-ended tube with a compact swirl flame at $x = x_q$ (see Figure 12). There is a jump at $x = x_q$ in mean temperature, from $\overline{T}_1$ to $\overline{T}_2$, and a corresponding jump in the mean density from $\overline{\rho}_1$ to $\overline{\rho}_2$ as well as in the speed of sound from c_1 to c_2. The flame is a compact swirl flame, burning methane in the lean combustion regime ($\phi = 0.77$). This configuration was studied in [24, 25], and the highlights are reported here.

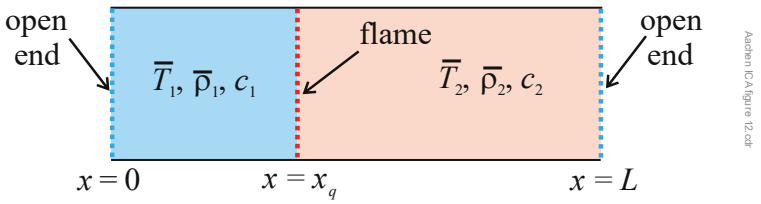

Figure 12 – Schematic illustration of the modelled configuration

The FDF was determined from CFD simulations [24]. An analytical approximation was found by the method described in Section 3, involving a superposition of two Gauss curves in the time domain,

$$q(t) = K\left[n_1 \int_{\tau=0}^{\infty} u_q(t-\tau)\, D_1(\tau)\, \mathrm{d}\tau - n_2 \int_{\tau=0}^{\infty} u_q(t-\tau)\, D_2(\tau)\, \mathrm{d}\tau \right], \tag{17}$$

with $K = \dfrac{\overline{Q}}{S\overline{u}_2\overline{\rho}_2}$ (this is a conversion factor between the local and global heat release rate; S is the cross-sectional are of the tube), and the distributions

$$D_1(\tau) = \frac{2}{\sigma_1\sqrt{2\pi}}\, e^{-\frac{(\tau-\tau_1)^2}{2\sigma_1^2}}, \quad D_2(\tau) = \frac{2}{\sigma_2\sqrt{2\pi}}\, e^{-\frac{(\tau-\tau_2)^2}{2\sigma_2^2}}. \tag{18}$$

The fitting parameters n_1, τ_1, σ_1 and n_2, τ_2, σ_2 were determined as described in Section 3. All of them turned out to decrease with amplitude. Their amplitude dependence was therefore approximated by the following linear functions (best fit),

$$n_1 = 7.4 - 14.94\frac{a}{\overline{u}}, \qquad n_2 = 4.7 - 14.94\frac{a}{\overline{u}} \tag{19}$$

$$\tau_1 = 4.13 - 6.56\frac{a}{\overline{u}}\,[\mathrm{ms}], \quad \tau_2 = 6.31 - 1.89\frac{a}{\overline{u}}\,[\mathrm{ms}] \tag{20}$$

$$\sigma_1 = 1.94 - 3.16\frac{a}{\overline{u}}\,[\mathrm{ms}], \quad \sigma_2 = 1.21 - 1.54\frac{a}{\overline{u}}\,[\mathrm{ms}] \tag{21}$$

The tailored Green's function was written as the sum of the first two resonator modes,

$$G(x, x^*, t-t^*) = \mathrm{H}(t-t^*)\left[G_1(x, x^*)\, \mathrm{e}^{-\mathrm{i}\omega_1(t-t^*)} + G_2(x, x^*)\, \mathrm{e}^{-\mathrm{i}\omega_2(t-t^*)} \right]. \tag{22}$$

The frequencies ω_1, ω_2 were calculated from an eigenvalue approach; they depend on the parameters c_1, c_2, x_q and L. The Green's function amplitudes, G_1, G_2, depend on the same parameters. Details can be found in [25].

By solving the integral equation (16) numerically with the time stepping method outlined in Section 4, the time history $u_q(t)$ was obtained over a long time interval, $t = [0,\ 10\mathrm{s}]$. This is shown in Figure 13; the relevant parameters are given in the figure caption.

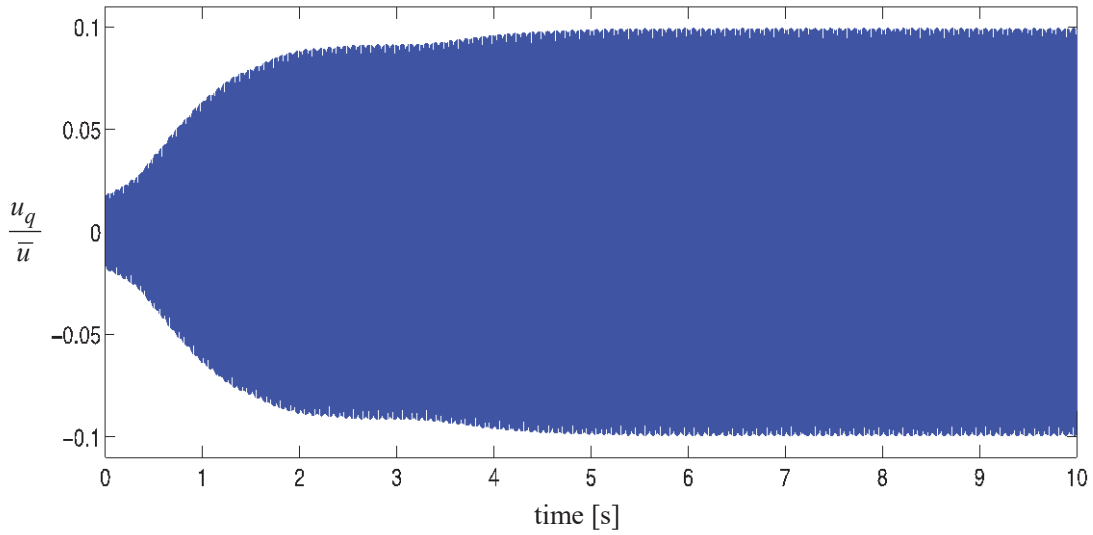

Figure 13 – Time history of $u_q(t)$ in an open-ended tube with length $L = 1.2\text{m}$ and flame at $x_q = 0.20\,\text{m}$; there is a cold region upstream (300 K for $0 \le x < x_q$) and a hot region downstream (1700 K for $x_q < x \le L$). The initial condition is $u_q(t=0)/\overline{u} = 0.01$; the Green's function includes the first two modes; the factor K was $K = 1.41\times10^6\,\text{W s kg}^{-1}$

The amplitude increases exponentially at first, and then grows less rapidly; beyond about $t = 2\text{s}$, a limit cycle is established with final amplitude $a/\overline{u} = 0.1$. In order to investigate whether or how the modal amplitudes change during the evolution, the frequency spectrum was calculated for an early time window, [0, 1s] (see Figure 14(a)), and for a late time window, [9s, 10s] (see Figure 14(b)). These spectra reveal that mode 1 is dominant during the growth stage of the evolution (small amplitudes), and that mode 2 takes over at the limit cycle stage (large amplitudes).

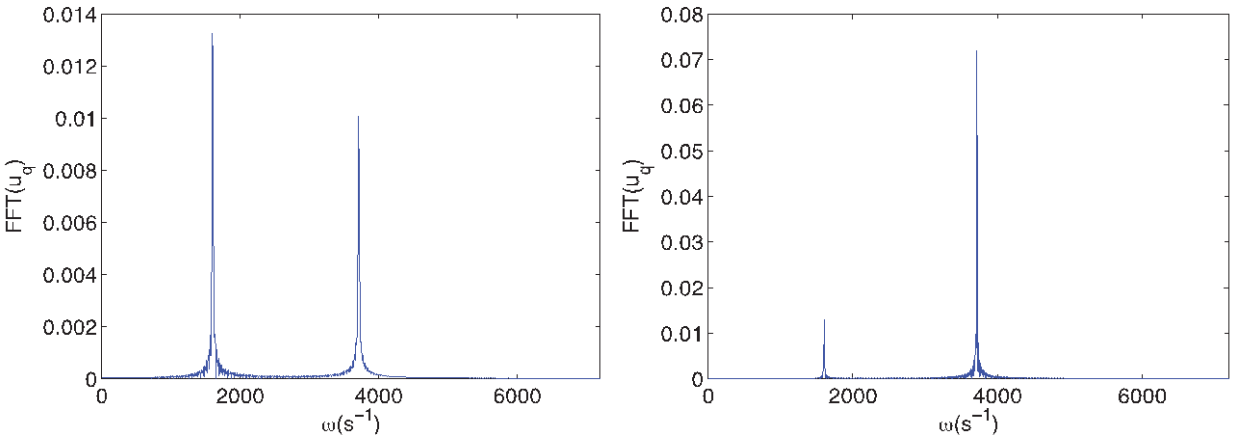

Figure 14 – Fourier transform of the time history shown in Figure 13.
(a) Time-window [0, 1s]. (b) Time-window [9s,10s].

6. CONCLUSIONS

This presentation has given an overview of the key physical mechanisms involved in thermoacoustic instabilities. At the core is a thermoacoustic feedback involving a flame in an acoustic resonator. In tandem with this primary feedback loop, there are secondary feedback loops; these involve low-Mach number transport processes perturbing the flame, which in turn emits an acoustic wave.

The two core elements of a low-order mathematical approach are a model for the flame and a model for the acoustic resonator. A method to model a flame analytically was introduced, based on experimental or numerical data for its flame describing function. This method is inspired by the physical fact that different transport processes are associated with different time-lags. Unsurprisingly, given this physics-inspired mathematical approach, the accuracy of the analytical flame models is very good and requires only a small number of fitting parameters.

Our model for the acoustic resonator is based on the tailored Green's function of that resonator. This is an uncommon approach; network models ending up in eigenvalue calculations are usually the method of choice for an analytical approach. However, the Green's function approach is more versatile. It can easily be combined with any flame model and predictions can be made, no matter whether the flame model is linear or nonlinear. The tailored Green's function is made up the actual *resonator modes*, so it is a natural tool for studying the interaction between two or more thermoacoustic modes. The most challenging part of this approach is the calculation of the tailored Green's function. However, once this has been determined for a particular configuration, a variety of scenarios can be simulated in a straightforward manner, and parameter studies can be made with a minimum of numerical effort. It is a very useful tool for designing new combustion systems that are immune to thermoacoustic instabilities.

REFERENCES

[1] Rijke, P.L. (1859) Notice of a new method of causing a vibration of the air in a tube open at both ends. *London Edinburgh and Dublin Philosophical Magazine and Journal of Science* 17, 419-422.

[2] Raun, R.L., Beckstead, M.W., Finlinson, J.C. & Brooks, K.P. (1993) A review of Rijke tubes, Rijke burners and related devices. *Progress in Energy and Combustion Science* 19, 313-364.

[3] Heckl, Maria A. (1985) *Heat sources in acoustic resonators*. PhD thesis, University of Cambridge.

[4] Lieuwen, T.C. & Yang, V. (2005) *Combustion instabilities in gas turbine engines*. American Institute of Aeronautics and Astronautics.

[5] Candel, S. (2002) Combustion dynamics and control: Progress and challenges. *Proceedings of the Combustion Institute* 29, 1-28.

[6] Lieuwen, T. (2003) Modeling premixed combustion-acoustic wave interactions: A review. *Journal of Propulsion and Power* 19, 765-781.

[7] Huang, Y. & Yang, V. (2009) Dynamics and stability of lean-premixed swirl-stabilized combustion. *Progress in Energy and Combustion Science* 35, 293-364.

[8] Poinsot, T. & Veynante, D. (2005) *Theoretical and numerical combustion, 2nd edition*. Edwards, Philadelphia.

[9] Culick, F.E.C. (2006) *Unsteady motions in combustion chambers for propulsion systems*. Research and Technology Organisation, NATO, RTO-AG-AVT-039.

[10] Heckl, Maria (2019) Advances by the Marie Curie project TANGO in thermoacoustics. *International Journal of Spray and Combustion Dynamics*, 11, 1-53.

[11] Hoeijmakers, M., Kornilov, V., Arteaga, I.L., de Goey, P. & Nijmeijer, H. (2014) Intrinsic instability of flame-acoustic coupling. *Combustion and Flame* 161, 2860-2867.

[12] Emmert, T., Bomberg, S. & Polifke, W. (2015) Intrinsic thermoacoustic instability of premixed flames. *Combustion and Flame* 162, 75-85.

[13] Silva, C.F., Emmert, T., Jaensch, S. & Polifke, W. (2015) Numerical study on intrinsic thermoacoustic instability of a laminar premixed flame. *Combustion and Flame* 162, 3370-3378.

[14] Chakravarthy, S.R., Sivakumar, R. & Shreenivasan, O.J. (2007) Vortex-acoustic lock-on in bluff-body and backward-facing step combustors. *Sadhana - Academy Proceedings in Engineering Sciences* 32, 145-154.

[15] Singh, G., Mariappan, S. & Singaravelu, B. (2017) Phase space dynamics of thermoacoustic interactions during vortex-acoustic lock-on. *Proceedings of the 24th International Congress on Sound and Vibration, London, UK, 23-27 July 2017*

[16] Marble, F.E. & Candel, S.M. (1977) Acoustic disturbance from gas non-uniformities convected through a nozzle. *Journal of Sound and Vibration* 55, 225-243.

[17] Goh, C.S. & Morgans, A.S. (2013) The influence of entropy waves on the thermoacoustic stability of a model combustor. *Journal of Sound and Vibration* 185, 249-268.

[18] Albayrak A, Bezgin DA & Polifke W. (2018) Response of a swirl flame to inertial waves. *International Journal of Spray and Combustion Dynamics*, 10, 277–286.

[19] Gopinathan, S.M. & Heckl, Maria (2019) Stability analysis and flashback limits for combustion systems using hydrogen blended fuels. *Proceedings if the 26th International Congress on Sound and Vibration, 7-11 July 2019, Montreal, Canada.*

[20] Noiray, N., Durox, D., Schuller, T. & Candel, S. (2008) A unified framework for nonlinear combustion instability analysis based on the flame describing function. *Journal of Fluid Mechanics* 615, 139-167.

[21] Howe, M.S. (1998) *Acoustics of fluid-structure interaction*. Cambridge University Press, Cambridge.

[22] Heckl, M.A. & Howe, M.S. (2007) Stability analysis of the Rijke tube with a Green's function approach. *Journal of Sound and Vibration* 305, 672-688.

[23] Bigongiari, A. & Heckl, M.A. (2016) A Green's function approach to the rapid prediction of thermoacoustic instabilities in combustors. *Journal of Fluid Mechanics* 798, 970-996.

[24] Iurashev, D., Campa, G. &. Anisimov, V. (2016) Response of swirl stabilized perfectly premixed flame to high-amplitude velocity excitations, *Proceedings of the 23rd International Congress on Sound and Vibration*, Athens, Greece, 10-14 July, 2016.

[25] Bigongiari, A. and Heckl, Maria (2018) Analysis of the interaction of thermoacoustic modes with a Green's function approach. *International Journal of Spray and Combustion Dynamics*, Vol. 10(4), pp. 326-336.